Neutral silicon interstitials in silicon carbide: a first principles study

Ting Liao, Guido Roma, Jingyang Wang

Neutral silicon interstitials in silicon carbide: a first principles study

Journal:	*Philosophical Magazine & Philosophical Magazine Letters*
Manuscript ID:	TPHM-08-Nov-0433.R1
Journal Selection:	Philosophical Magazine
Date Submitted by the Author:	20-Jan-2009
Complete List of Authors:	Liao, Ting; IMR, High Performance Ceramic Division; CEA-Saclay, Service de Recherches de MÃ©tallurgie Physique Roma, Guido; CEA-Saclay, Service de Recherches de MÃ©tallurgie Physique Wang, jingyang; IMR, High Performance Ceramic Division
Keywords:	defects, diffusion, first-principles calculations, silicon carbide
Keywords (user supplied):	defects, diffusion, first-principles calculations

Neutral silicon interstitials in 3C- and 4H-SiC: A first-principles study

Ting Liao[1,2,3], Guido Roma[1,*] and Jingyang Wang[2]

1 Service de Recherches de Métallurgie Physique, CEA Saclay, 91191 Gif sur Yvette, France

2 High-performance Ceramic Division, Shenyang National Laboratory for Materials Science, Institute of Metal Research, Chinese Academy of Sciences, Shenyang, 110016, China

3 Graduate School of Chinese Academy of Sciences, Beijing, 100039, China

Abstract. The structures and stability of single silicon interstitials in their neutral state are investigated via first principles calculations in 3C- and 4H-SiC. By carefully checking the convergence with Brillouin Zone (BZ) sampling and supercell size we explain the disagreement between previous published results and we show that the split interstitial along <110> direction and tetrahedrally carbon coordinated structure have competing formation energies in the cubic polytype. A new migration mechanism for the silicon interstitial in the neutral state is presented here which could be important for the evolution of defect populations in SiC. For 4H-SiC, the most energetically favourable silicon interstitial is found to be the split interstitial configuration $I_{Sisp<110>}$ but situated in the hexagonal layer. The defect formation energies in 4H-SiC are in general larger than those in 3C-SiC, implying that the insertion of silicon interstitial introduces a large lattice distortion to the local coordination environments and affect even the second- or third-nearest neighbours. We also present a comparison between well converged plane waves calculations and calculations with three localized orbital basis sets; one of them, in spite of providing a reasonable description for bulk properties, is clearly not suitable to describe interstitial defects.

Keywords: Defects, Diffusion, First principles calculations, silicon carbide

1. Introduction

Silicon carbide (SiC) is a wide band-gap semiconductor ideally suited for high-temperature, high-power, and high-frequency applications [1], and its composites have been proposed for

* Corresponding author

structural components in future nuclear fusion reactors [2, 3], because of their high temperature strength, pseudo-ductile fracture behaviour, and low-induced radioactivity. In order to assess the performance of SiC-based components in radiation or ion implantation environments, a detailed understanding of the influence of defects on their structure and behaviour is necessary.

Other domains of the application of silicon carbide include very high temperatures and irradiation environments where, in spite of their relatively high formation energies, silicon interstitials are expected to be present in high concentrations and will be important, maybe even crucial, in order to understand the behaviour of the material and its evolution. Indeed their mobility is expected to be high and they may play an important kinetic role [4] in the microstructural evolution. Furthermore, the amorphous SiC created by irradiation is known to include a large percentage of homopolar bonds, but its details are not yet fully understood [5-7].

Theoretical studies of point defects in SiC have been widely performed using accurate density functional theory (DFT) [4,8-13], but relatively few studies regarding silicon interstitials have been published so far [4,10-12]; furthermore, some discrepancies between published results need a clarification. Indeed, depending on the variation of supercell size and *k*-point sampling, different formation energies have been reported so far for silicon interstitials in SiC. Defect energies calculated from DFT are expected to be quite accurate, nevertheless in several cases it has been shown that a higher level of theory than for the description of the bulk material is necessary [14-15]. We noticed that in the cited studies for silicon interstitials, in spite of different cell sizes used, the *k*-point samplings are almost all limited to the Γ point. Our results show that, even for supercells larger than all those used up to know, Γ point sampling is a source of large errors. In addition, our extensive comparison of plane waves based calculations with localised orbitals based ones shows that discrepancies can be non negligible on formation energies. Finally, we have found a mechanism for migration of the neutral silicon interstitial whose migration barrier is lower than previously reported.

The paper is organized as follows: the computational details are described in section 2. In section 3 we present results for the formation energies of silicon interstitials in both 3C- and 4H-SiC. The dependence of the defect formation energy on the *k*-point choice and supercell

size, along with the description of local coordination environments of each interstitial type, is also illustrated in this section, as well as the migration mechanism in 3C-SiC. Finally, the concluding remarks are given in section 4.

2. Computational details

To determine the relative stability of different interstitial configurations, we compared their defect formation energies and, for this, we follow the standard formalism outlined in several previous studies to define reasonable bounds on the chemical potentials and to investigate the defect energies within these limits [16-18]. As a reminder, the formation energy of a neutral defect in SiC is hence defined as

$$E_f = E_{def} - n_{Si}\mu_{si} - n_C\mu_C \quad (1)$$

Here, the chemical potentials μ_i are not independent μ_{SiC} but related to the chemical potential of bulk SiC, , i.e., $\mu_{Si} + \mu_C = \mu_{SiC}$, and n_i is the number of atoms of type *i* added or removed to form the defect.

E_{def} is the difference in energy beween the supercell with and without the defect.

The analysis of the silicon interstitials was carried out by means of total energy calculations within the framework of Density Functional Theory (DFT), and by simulating the relevant interstitials using periodic supercells containing 64 and 72 atoms, respectively, for 3C- and 4H-SiC. We also enlarged the supercells of 3C-SiC to 128-, 216- and 512-atom to investigate the effects of the choices of supercell sizes as well as the *k*-point sampling on the results. The energies and forces calculations were performed using two codes with different basis sets, PWSCF (Plane Wave Self Consistent Field) using plane waves [19] and SIESTA (Spanish Initiative for Electronic Simulations with Thousands of Atoms) with linear combination of atomic orbitals [20]. In plane-wave PWSCF calculations we used ultrasoft and norm-conserving pseudopotentials to replace the core electrons of C and Si atoms, respectively. In most of the calculations, to provide sufficiently well-converged results, a 2×2×2 shifted Monkhorst-Pack

k-point mesh was used for the sampling of the Brillouin Zone. The exchange correlation energy is calculated in the Local Density Approximation (LDA). We employed a plane-wave cutoff energy of 30 Ry for energy calculations which is sufficient to achieve a full convergence of 2×10^{-2} eV/atom on total energies. We found no need to raise the charge density cutoff above 120 Ry. The atomic positions are relaxed until the Hellman-Feynman force on each atom is reduced to within 10^{-3} Ry/Bohr (2.6×10^{-2} eV/Å).

SIESTA calculations were also done within LDA for bulk and defected structures. The core electrons were replaced by norm-conserving pseudopotentials generated by Troullier and Martins[21]; valence electrons were described by three basis sets: a double-ζ polarized (DZP) basis set, a triple-ζ one without polarization (TZ), and a triple-ζ basis set including polarization for silicon orbitals (TZP) [22].

Deleted: Troullier-Martins

Deleted: according to the recipe

More details for the comparison of the basis sets, including equilibrium bulk properties, are in table 1. A 2×2×2 shifted *k*-points mesh and 80 Ry grid cutoff were adopted for all energy calculations, unless stated otherwise. The convergence tolerance for the geometry optimization was a maximum Hellmann-Feynman force within 0.01 eV/Å.

3. Results and discussion

3.1. Formation energy and convergence issues for silicon interstitials in 3C-SiC

The crystallographic structure 3C-SiC is of the zinc-blend type; it consists of zigzag chains when regarded along the <110> direction and it can be described as a stacking of atomic planes with hexagonal symmetry in the sequence of ABCABC along the <111> axis of the conventional cubic cell. For the modelling of the interstitial defects in this type of structure, we place the interstitial atoms in the regions with open space and in the form of split-interstitial configurations distinguished by the crystallographic symmetry and the local environments (see red balls in figure 1), and perform relaxation to allow for the minimization of the forces and stresses. As depicted in figure 1, different starting interstitial configurations have been explored for 3C-SiC: the tetrahedrally coordinated interstitial sites, with either a four silicon (I_{TSi}) or four

carbon (I_{TC}) nearest neighbors; a hexagonal configuration I_{Hex}, where the interstitial atom is located in the center of a hexagon of alternating silicon and carbon atoms; various split interstitial configurations sharing either carbon or silicon lattice site, occurring with orientations in the <100>, the <110> and the <111> directions; furthermore we considered a bond-center configuration where the interstitial silicon is centered at the heteropolar bond of two nearest neighbouring lattice atoms.

The calculated results of the silicon interstitial formation energies of 3C-SiC in the two extreme chemical potential conditions are tabulated in table 2. The results in here are obtained by variable-cell optimization, which partially relieves the elastic energy arising from the crystallographic distortion induced by the defect. The ordering according to formation energy of the various configurations is the same for the PWSCF plane waves calculations and the SIESTA with basis sets DZP and TZP. The TZ unpolarized basis set gives much higher formation energies. In the following we will mainly comment on SIESTA calculation with the DZP basis, as they are more efficient than the TZP and give results which are almost as close to the PW results as the TZP ones. As can be seen from table 2, silicon interstitials in 3C-SiC respond strongly to the different local coordination environments and the hierarchy of silicon interstitials also depends on it. Here, the most stable configuration is the dumbbell-like split interstitial on a silicon site along <110> direction (E_f = 8.40 eV) followed by the tetrahedrally carbon-coordinated interstitial I_{TC} (E_f = 8.98 eV). We refer to formation energies in silicon rich conditions, unless stated otherwise. This result is in disagreement with prior calculations also using plane-wave pseudopotential methods [10-11], which find I_{TC} to be the most favourable Si interstitial (E_f = 6.00 eV) and obtain for the $I_{Sisp<110>}$ a formation energy which is 1.40 eV higher. We noticed that the two calculations, using 128 and 64 atom supercells respectively, both sampled the Brillouin-zone with the Γ point only. The work by Salvador *et al* [12], with a larger supercell containing 216 atoms, still with Γ point sampling, gives a formation energy of 6.7 eV for the carbon-coordinated interstitial I_{TC}, consistent with the result from Lento et al., and suggesting a well converged result in these works, at least under the Γ point sampling condition. However, by employing a 64-atom cell and a denser *k*-point sampling (2×2×2 shifted mesh), an

agreement can be found on the formation energies of $I_{Sisp<110>}$ in the neutral state between our results and those from M. Bockstedte *et al* [4]. All the cited works are results of plane waves pseudopotential calculations.

More recently it has been shown that in semiconductors, like silicon and diamond, even if energy differences are calculated between values obtained with equivalent supercell sizes and *k*-point sampling, the error in formation energies caused by the limitation of *k*-point sampling will not be easily cancelled out [23]. It is thus necessary to check the effect of the choice of *k*-point sampling on the energy convergence of defect-containing structures. It is worth restating that we are using supercells in order to simulate an isolated defect. The fact that *k*-point sampling of the BZ has to be carefully considered comes from two reasons: first, the screening in the bulk material has to be correctly described; second, the defect levels themselves can show a dispersion with *k*. The latter means that our defect periodic images are interacting and there is an error coming from the finite size of the supercell, in spite of the convergence with *k*-point sampling.

In figure 2a, we compare the convergence of defect formation energies of I_{TC} and $I_{Sisp<110>}$ in 3C-SiC structures in terms of different *k*-point samplings for the 65- and 129-atom supercells with fully relaxed atomic positions at constant volume. Here, we obtained a formation energy for I_{TC} in close agreement with the value from Lento *et al*. based on the same calculation conditions (at Γ point and for 128-atom supercell). As shown in figure 2a, the convergence with increasing *k*-point density is slow and, in particular, the formation energy for $I_{Sisp<110>}$ defect converge more quickly than the interstitial I_{TC} does; in other words, the latter defect responds more sensitively to the choice of *k* points. With increasing *k* grid density, the formation energies of I_{TC} and $I_{Sisp<110>}$ finally converged at 8.92 and 8.67 eV, in a 128 atoms supercell.

We also remark that, as suggested previously [24], the only fact of using another *k*-point —(½,½,½) for cubic cells and (¼,¼,¼) for FCC cells)— instead of Γ allows to obtain almost converged values.

We now discuss the other main source of error, which is the limited size of the supercell. We performed the atomic relaxation of the I_{TC} and $I_{Sisp<110>}$ structures considering both Γ only and

converged k-point samplings, respectively, by increasing the cell size up to 512-atom. The results are shown in figure 2b. As the size of the supercell increases the formation energies for both defect configurations calculated using the Γ-point sampling increase significantly. When converged with respect to the *k*-point sampling the formation energy for the split configuration seems well converged already with a 65 atoms supercell, but for the tetrahedral one the energy still decreases, reminding of the case of the vacancy in silicon [23].

This behaviour can be rationalized by a closer look into the electronic structure of these defects. Indeed the T_C position, in the 65 atoms supercell, has occupied levels above the conduction band edge, which means that the system becomes metallic (or that this defect is expected to be positively charged at any doping condition). This effect could be an artifact of the well known underestimation of the band gap by DFT-LDA calculations. In some cases in which the DFT band structures are even qualitatively different from experimental excitations spectra, total energies and structural properties are relatively well described. Let us mention the example of a Mott insulator: uranium dioxide [25]. However our findings warn about the possible errors of standard DFT approaches even for neutral defects in solids whose ground state properties are believed to be relatively well described. In conclusion, the interstitials configurations I_{TC} and $I_{Sisp<110>}$ are very close in formation energy and separated by at most a few tenth of an eV, in DFT-LDA. Our best converged results (8.12 and 8.27 eV respectively) were obtained with a 512-atom supercell and 2×2×2 shifted *k*-point mesh.

Deleted: However, i

Deleted: everal

Deleted: .

The split interstitials at silicon site with <100> and <111> orientations have higher formation energies than I_{TC} and $I_{Sisp<110>}$, and the tetrahedrally silicon-coordinated interstitial I_{TSi} turns out to be the least stable one in all investigated interstitial configurations. These three configurations, which have metallic character as I_{TC}, are either very shallow minima or even saddle points, because a very small perturbation, releasing the symmetry constraints, allows the configuration to switch to the $I_{Sisp<110>}$ configuration with practically no barrier. These three almost unstable configurations can then provide migration mechanisms with migration energies (1.5-2.5 eV) similar or higher than those reported by Bockstedte [4] for neutral species.

The effect of the insertion of silicon interstitials on the relative volume changes after relaxation

is also presented in table 2. The interstitials in the split-interstitial form produce a comparatively larger expansion of the crystalline volume and such distortion make the defects less symmetric, whereas others, such as the carbon- and silicon-coordinated interstitial configuration, have a much smaller effect and their volume expansion after a full relaxation was 0.99 % and 1.29 %, respectively. This suggests that the slow convergence with cell size for I_{TC} is not related to the elastic interactions between defect periodic images. SIESTA calculations yields in general slightly larger volumes expansion, and even much larger for the TZ basis sets (up to more then four atomic volumes).

3.2. Local environments of silicon interstitials in 3C-SiC

In table 2, interstitial atoms and the nearby atoms are shown at relaxed positions for 3C-SiC, including a summary of relaxed local bond lengths for the interstitials. The criterion for bonding is chosen to be the atomic distances with the upper thresholds of 2.40 Å for Si-Si bonds and 1.90 Å for Si-C bonds. Although supercells of each type dilate accordingly with the silicon insertion, the changes in bond lengths for each defect have to be understood in terms of local coordination environments and charge effects. For the tetrahedrally coordinated interstitials surrounded by carbon or silicon atoms, T_d symmetry is kept, with some differences from the relaxation pattern of the nearest atoms. For I_{TSi}, the nearest silicon atoms move slightly away from the interstitial site, whereas in I_{TC} the four carbon first neighbours move slightly closer. The tetrahedron formed by these carbon atoms undergoes a volume contraction of around 7%, while the octahedron formed by the six silicon second-neighbours get strongly dilated (~30% in volume). The latter constitutes the main contribution to the volume expansion induced by the T_C interstitial.

Due to the open structure of the SiC along the <110> direction, the split interstitial configuration with this orientation can easily release the strain energy. The starting configurations with split interstitials at carbon site along <110> and <111> directions and with the silicon atom residing in the center of a hexagon of alternating silicon and carbon atoms are unstable, and they all relax

down to the tetrahedrally carbon-coordinated symmetry ultimately. Besides all these well documented silicon interstitial configurations, another different point defect pattern in the form of a combination of antisite Si_C plus a carbon split interstitial I_{CspSi} on a silicon site was also found in our study. This result was obtained with a slight torsion of the Si-C bonds surrounding the hexagonal interstitial site, and a three-membered ring was formed encircled by the antisite defect and the split pair. This defect complex is also a relatively low-energy defect structure of silicon interstitial with a formation energy equal to 9.27 eV (Si-rich conditions). Compared to the others silicon interstitial structures, this defect complex is only less stable than the I_{TC} and $I_{Sisp<110>}$, and could play a role in the energy landscape of silicon interstitials.

3.3. A mechanism for the migration of silicon interstitials in 3C-SiC

Interstitial mobility is known to be higher than that of vacancies in SiC [4]. In the presence of Si self-interstitials, the identified almost equally stable configurations, I_{TC} and $I_{Sisp<110>}$, might transform into one another by thermal activation. We estimated the barrier of this transition by searching the minimum energy path between I_{TC} and $I_{Sisp<110>}$ in their neutral state. The path, generated using the nudged elastic band (NEB) [26] method as implemented in PWSCF, is depicted in figure 3 for the 4x4x4 FCC supercell (containing 128 atoms). The process which transforms I_{TC} into $I_{Sisp<110>}$ and vice versa is not exceeding 0.85 eV. As an approximate evaluation of the error due to supercell size limitation for the migration barrier we have calculated the energy path with and without smearing of the Fermi surface; the difference of the two curves at the saddle point is of 0.1 eV. The influence of the smearing of the Fermi surface, for which we adopted the cold-smearing scheme proposed by Marzari and coworkers [27], is negligible: for the I_{TC} configuration, the calculated result with a smearing width of 0.005 Ry (presented in figure 3) differs by 0.02 eV with respect to the one with a smearing of 0.0001 Ry.

We performed further calculations with a 217 atoms cubic supercell that confirm a migration energy between 0.7 and 0.8 eV. For this migration path, starting with I_{TC} , the silicon interstitial begins with a hop away from the tetrahedral interstice and pushes the nearby silicon atom out of its normal site to form a distorted intermediate split interstitial in a direction close to <100>.

Formatted: Subscript
Deleted: ion
Deleted: r
Deleted: ,

After this, a collective displacement of these two atoms toward the final $I_{Sisp<110>}$ dumb-bell takes place, until equilibrium is reached, while all other atoms relax only slightly during the diffusion event. To the best of our knowledge this migration mechanism of neutral silicon interstitials has definitely the lowest activation energy than all the previously reported ones [4]; it should be the dominant mechanism for Si self-diffusion in compensated and *n*-type SiC, according to the charge transition levels calculated in [4].

3.3. Relative stability of silicon interstitials in 4H-SiC

The crystal structure of 4H-SiC can be described as the alternating cubic and hexagonal stacking sequence arranged along c-axis in a form of ABCBABCB. The higher number of non-equivalent lattice sites in 4H-SiC leads to a greater variety of potential elementary interstitial defect than in 3C-SiC. Having recognized the instability of silicon split-interstitial on carbon site for 3C-SiC, we did not consider this insertion site in 4H-SiC. The investigated initial silicon interstitial configurations in 4H-SiC are all displayed in figure 4. As in 3C-SiC the cubic lattice layer enclose both the tetrahedrally carbon and silicon coordinated sites. In the hexagonal layer, interstitial site I_{TCSi} is characterized by a tetrahedral surrounding by four carbon and four silicon atoms, and $I_{Hex(CSi)}$ is in an open cage encompassed by two hexagonal rings of the lower and upper basal plane. Another hexagonal configuration I_{Hex}, which resembles that in 3C-SiC is located in the center of a hexagon of alternating silicon and carbon atoms. For the split interstitials in 4H-SiC, they can be located entirely within a basal plane considering different orientations of $<10\bar{1}0>$ or $<1\bar{2}10>$.

In addition, other split interstitial configurations resembling the crystallographic geometry in 3C-SiC along <100> or <110> directions are also taken into account. All the split interstitial patterns apply to the lattice sites in the cubic layer as well as in the hexagonal layer.

Table 3 summarizes the calculated formation energy of all investigated stable interstitials in 4H-SiC for C- and Si-rich limits. They were obtained with a 3x3x1 supercell containing 72(+1) atoms and 3x3x1 *k*-point mesh. The most energetically favourable interstitial configuration in

4H-SiC is the split interstitial with <110> orientation on the silicon atom site, which locates in the hexagonal layer.

A similar Si-Si split with the same orientation in the cubic region turns out to be less stable by 0.87 eV. In particular, this split pair in the cubic layer provokes stronger distortion of the simulation supercell and induces a larger volume expansion by 0.3 % than the pair does in the hexagonal region. On the basal plane, split interstitials along $<10\bar{1}0>$ and $<1\bar{2}10>$ crystallographic orientations result in different interstitial configurations. Both dumbbell configurations with $<10\bar{1}0>$ symmetry in cubic and hexagonal planes exhibit almost identical stability due to the similar nearest-neighbour environments which allow for similar relaxation pattern. Their defect formation energies differ from one another negligibly, although a switch of comparative orders is observed changing from the TZP basis set (in agreement with plane waves) to the DZP or TZ basis sets. In the cases of $<1\bar{2}10>$-oriented configurations, even without a perturbation, these two split interstitials turn out to be very unstable and re-orientate their directions into <100> and <110>, respectively, in cubic and hexagonal layers. Let us emphasize that the <100> orientation, which turned out to be metallic in the cubic polytype, has its highest occupied band inside the gap, thanks to the larger band gap of 4H-SiC. We expect then, in general, the size effect to be much smaller for the 4H polytype than for the 3C. I_{TCcub}, which is characterized by a tetrahedral site surrounded by four carbon atoms in the cubic layer, is the least favourable stable configuration in 4H-SiC and is unstable if relaxed with SIESTA and the TZ basis set. The two other tetrahedral configurations, I_{TCSi} and I_{TSicub}, turn out to be unstable.

When comparing the relaxed structures of the interstitial atoms and their nearby atoms in 4H-SiC, as shown in table 3, we notice that, despite the complexity of non-equivalent lattice site, many relaxed interstitial structures share the same spatial symmetry characteristics, for example, the obtained stable split-interstitial configurations all have a symmetry of C_s, and the others are classified into the pattern C_{3v} holding the most typical three-axis rotation symmetry in hexagonal 4H-SiC. It is also interesting to notice that the relaxed positions of silicon interstitial

in the hexagonal region encompassed by two hexagonal rings, which are named as I_{Hex} and $I_{Hex(CSi)}$, are so close to one another that, with a tiny perturbation the less stable configuration I_{Hex} will change to $I_{Hex(CSi)}$ with great ease by sliding down the potential energy surface.

4. Conclusions

The energies of silicon interstitials in 3C- and 4H-SiC have been calculated from first principles by exploring a variety of possible configurations. The stable interstitial configurations have been characterized by formation energies and formation volumes.

We clarified that discrepancies between previously published results are due to limitations in supercell size and/or *k*-point sampling. In particular, the determination of the most stable position of the neutral silicon interstitial in cubic SiC is very delicate, showing a competition between the split interstitial sharing a silicon lattice site along <110> orientation and the tetrahedral position surrounded by carbon atoms. In the hexagonal polytype the former is clearly the most stable position. The formation energies for the most stable configurations are all above 8 eV.

The comparison between the two polytypes (3C and 4H) shows similar formation energies, in general higher for the hexagonal polytype, if we compare similar configurations. We also compare well converged results obtained with a plane waves basis sets with the outcome of SIESTA calculations using different localized basis set. The best compromise seems to be a double-ζ polarized basis set. The stability order of the various configurations is almost always the same as with plane waves, the formation energies are similar, but the differences can be as large as 0.5 eV. The SIESTA calculations give lower formation energies than plane waves for the 4H polytype but higher than plane waves for the cubic one. Nevertheless the trend showing higher formation energies in the hexagonal polytype is maintained.

We have found a diffusion mechanism for the silicon interstitial in cubic SiC, consisting in hops between split and tetrahedral configurations; the corresponding migration energy is estimated at 0.8 eV, lower than previously reported ones [4]. This point suggests that silicon interstitials

could play a role more important than expected in the evolution of defects populations in SiC under irradiation.

Acknowledgements

We are grateful to Yanchun Zhou and the Institute of Metal Research (Shenyang, China) for making possible the one year stay of T.L. at CEA-Saclay during her PhD period in the framework of the collaboration between our two laboratories. We also wish to acknowledge the support of CCRT (Centre de Calcul de Recherche et Technologie) for the computing time allocated through the parternership with CEA Nuclear Energy Division (DEN).

References

[1] S. Dimitrijev and G. Jamet G, Microelectron. Reliab. 43 (2003) p.225-233

[2] G. R. Hopkins *Silicon Carbide and Graphite Materials for Fusion Reactors* Proc. IAEA Symp. Plasma Phys. and Controlled Nucl. Fusion Res., Tokyo, Japan, International Atomic Energy Agency IAEA-CN-33/s3-3, 1974.

[3] A. Hasegawa, A. Kohyama, R.H. Jones, L. L. Snead, B. Riccardi and P. Fenici, J. Nucl. Mater. 283 (2000) p.128-137

[4] M. Bockstedte, A. Mattausch and O. Pankratov, Phys. Rev. B 68 (2003) p.205201

[5] M. Ishimaru, I. T. Bae, A. Hirata, Y. Hirotsu, J. A. Valdez and K. E. Sickafus, Nucl. Instrum. Meth. Phys. Res. B 242 (2006) p.473-475

[6] M. Ishimaru, I. T. Bae, Y. Hirotsu, S. Matsumura and K. E. Sickafus, Phys. Rev. Lett. 89 (2002) p.055502

[7] R. Devanathan, F. Gao and W. J. Weber, Appl. Phys. Lett. 84 (2004) p.3909-3911

[8] A. Mattausch , M. Bockstedte and O. Pankratov, Phys. Rev. B 69 (2004) p.235202

[9] A. Mattausch, M. Bockstedte and O. Pankratov, Mater. Sci. Forum 457-460 (2004) p.449

[10] J. M. Lento, L. Torpo, T. E. M. Staab and R. M. Nieminen, J. Phys.: Condens. Matter 16 (2004) p.1053-1060

[11] E. J. Bylaska, K. Tsemekhman and F. Gao, Phys. Scr. T124 (2006) p.86-90

[12] M. Salvador, J. M. Perlado, A. Mattoni, F. Bernardini and L. Colombo, J. Nucl. Mater. 329-333 (2004) p.1219-1222

[13] T. T. Petrenko, T. L. Petrenko and V. Y. Bratus, J. Phys.: Condens. Matter 14 (2002) p.12433-12440

[14] A. Janotti and C. G. Van de Walle, Appl. Phys. Lett. 87 (2005) p.122102

[15] J. Lægsgaard and K. Stokbro, Phys. Rev. Lett. 86 (2001) p.2834-2837

[16] S. B. Zhang and J. E. Northrup, Phys. Rev. Lett. 67 (1991) p.2339-2342

[17] S. B. Zhang, S. H. Wei and A. Zunger, Phys. Rev. B 57 (1998) p.9642-9456

[18] A. F. Kohan, G. Ceder, D. Morgan and C. G. Van de Walle, Phys. Rev. B 61 (2000) p.15019-15027

[19] Giannozzi P *et al*. http://www.quantum-espresso.org

[20] J. M. Soler *et al*., J. Phys.: Condens. Matter 14 (2002) p.2745-2779

[21] N. Troullier N and J. L. Martins, Phys. Rev. B 43 (1991) p.1993-2006

[22] J. Junquera, O. Paz, D. Sánchez-Portal and E. Artacho, Phys. Rev. B 64 (2001) p.235111

[23] J. Shim, E. K. Lee, Y. J. Lee and R. M. Nieminen, Phys. Rev. *B* 71 (2005) p.245204

[24] G. Makov, R. Shah and M. C. Payne, Phys. Rev. B 53 (1996) p.15513-15517

[25] J. P. Crocombette, F. Jollet, L. Thien Nga and T. Petit, Phys. Rev. B 64 (2001) p.104107

[26] G. Henkelman, B. P. Uberuaga, H. Jonsson, J. Chem. Phys. 113 (2000) 9901-9904

[27] N. Marzari *et al*., Phys. Rev. Lett. 82 (1999) p.3296-3299

[28] A. Mattausch, Ph. D. Thesis, Friedrich-Alexander-Universität Erlangen-Nürnberg (2005)

Formatted: Font: Italic

Deleted: [27]

Deleted: ¶
¶
¶
¶
¶
¶

Table 1. Comparison of results for bulk cubic SiC and for two interstitials configurations obtained with plane waves and with three different local orbital basis sets (see the text for details). The (Si-rich) formation energies were calculated with 65 atoms supercells and full atomic positions and cell volume relaxation.

Basis set	Energy shift	Mesh Cutoff	A0 [Bohr]	B0 [kbar]	E_f ($ISi_{sp<110>}$) [eV]	E_f (ISi_{TC}) [eV]
Localised DZP	0.34 eV	80 Ry	8.23	2256	8.6	9.6
Localised TZ	0.10 eV	90 Ry	8.28	2226	10.7	13.4
Localised TZP	0.05 eV	90 Ry	8.16	2223	8.6	9.2
Plane Waves	-	-	8.21	2230	8.4	9.0

Formatted: Font: Italic

Formatted: Font: Italic

Deleted: ¶

Deleted: ¶

Formatted: Line spacing: Double

Table 2. Summary of silicon interstitials in order of decreasing relative stability for 3C-SiC, including the relaxed structure, the relevant bond lengths and the relative volume changes of the supercell (Ω), the crystallographic symmetry and their formation energies under C-rich and Si-rich conditions. [a] plane waves (PWSCF code) [b] (localised orbitals) SIESTA code [c] Lento *et al.* [7] [d] Bylaska *et al.* [8] [e] Bockstedte *et al.* [6] [f] Salvador *et al.* [9]

Defect	Structure	Distance (Å)	E_f (C-rich) (eV)	E_f (Si-rich) (eV)	$\Delta\Omega$ (%)	Symmetry
$I_{Sisp<110>}$	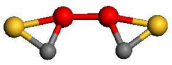	$(Si\text{-}Si)_{sp}$:2.13; Si-Si:2.31 Si-C:1.77	8.86[a]	8.40[a]	1.85[a]	C_{2v}
			9.12[b]	8.59[b]	2.29[b]	
				7.4[c]		
				8.5[e]		
I_{TC}		Si-C:1.84	9.43[a]	8.98[a]	0.99[a]	T_d
			10.07[b]	9.55[b]	1.28[b]	
				6.0[c]		
				7.65[d]		
			7.34[f]	6.70[f]		
$I_{Sisp<100>}$		$(Si\text{-}Si)_{sp}$:2.03; Si-C:1.79	10.23[a]	9.78[a]	2.43[a]	D_{2d}
			10.42[b]	9.90[b]	2.84[b]	
				9.83[d]		
$I_{Sisp<111>}$	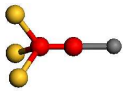	$(Si\text{-}Si)_{sp}$:2.06; Si-Si:2.24 Si-C:1.71	11.04[a]	10.58[a]	1.62[a]	C_{3v}
			11.41[b]	10.88[b]	2.05[b]	
I_{TSi}		Si-Si:2.17	11.30[a]	10.85[a]	1.29[a]	T_d
			11.75[b]	11.22[b]	1.60[b]	
				8.4[c]		
				7.84[d]		
			9.45[f]	8.81[f]		

Table 3. Summary of silicon interstitials for 4H-SiC, from most to less stable, including the relaxed structure, the relevant bond lengths and the relative volume changes, the crystallographic symmetry and their formation energies under C-rich and Si-rich conditions.
[a] plane waves (PWSCF code) [b] localised orbitals(SIESTA code) [c] Mattausch [28]

Defect	Structure	Distance (Å)	E_f (C-rich) (eV)	E_f (Si-rich) (eV)	$\Delta\Omega$ (%)	Symmetry
$I_{sp<110>hex}$	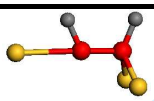	$(Si\text{-}Si)_{sp}$:2.15; Si-Si:2.34; Si-C:1.77	10.05[a]	9.57[a]	2.15[a]	C_s
			9.51[b]	8.99[b]	2.08[b]	
				9.03[c]		
$I_{sp<10\bar{1}0>cub}$	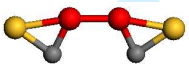	$(Si\text{-}Si)_{sp}$:2.10; Si-Si:2.27; Si-C:1.77	10.60[a]	10.12[a]	2.22[a]	C_s
			10.08[b]	9.56[b]	2.20[b]	
$I_{Hex(CSi)}$	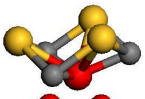	Si-C:1.87; Si-Si:2.30	10.61[a]	10.13[a]	1.82[a]	C_{3v}
			10.19[b]	9.67[b]	1.81[b]	
$I_{sp<10\bar{1}0>hex}$	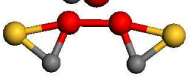	$(Si\text{-}Si)_{sp}$:2.12; Si-Si:2.25; Si-C:1.79	10.67[a]	10.19[a]	2.28[a]	C_s
			10.08[b]	9.55[b]	2.23[b]	
I_{Hex}	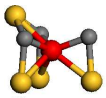	Si-C:1.86-1.87; Si-Si:2.32-2.34	10.77[a]	10.30[a]	1.82[a]	C_{3v}
			10.39[b]	9.86[b]	1.81[b]	
$I_{sp<110>cub}$	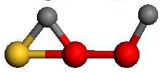	$(Si\text{-}Si)_{sp}$:2.01; Si-Si:2.28; Si-C:1.74-1.78	10.92[a]	10.44[a]	2.46[a]	C_s
			10.39[b]	9.87[b]	2.37[b]	
				9.37[c]		
$I_{sp<100>cub}$		$(Si\text{-}Si)_{sp}$:2.02; Si-C:1.76-1.83	11.19[a]	10.71[a]	2.67[a]	C_s
			10.66[b]	10.14[b]	2.61[b]	
I_{TCcub}	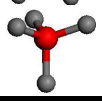	Si-C:1.83-1.86	12.12[a]	11.64[a]	1.52[a]	C_{3v}
			11.98[b]	11.46[b]	1.53[b]	

Figure 1 (Colour online) The investigated initial configurations of silicon interstitials in 3C-SiC (The split interstitials on carbon site are not displayed for brevity). The <111> direction is normal to the page.
From left to right: I_{TSi} I_{Cent} I_{TC} $I_{Sisp<100>}$ $I_{Sisp<110>}$ $I_{Sisp<111>}$ $I_{Hex(side+front)}$

Figure 2 (Colour online) Convergence of the formation energy of two types of silicon interstitials, I_{TC} and $I_{Sisp<110>}$, in 3C-SiC with respect to different k-point samplings (a) (n+1/2 x values corresponds to shifted k-point meshes), for the 65- and 129-atom supercells; convergence with respect to the increasing cell sizes (b), for Γ and converged k-points mesh, respectively.

Figure 3 Energy path for the migration from $I_{Sisp<110>}$ to I_{TC} (from left to right) in 3C-SiC. Empty symbols represent points calculated with smearing of the Fermi surface, filled symbols were calculated with filled occupations. Lines are a guide to the eye.

Figure 4 (Colour online) The investigated initial configurations of silicon interstitials in 4H-SiC. Configurations labels from left to right follow. <1$\underline{2}$10> direction is normal to the page.
Cubic (upper) layer: I_{TSicub} I_{TCcub} $I_{Sisp<100>}$ $I_{Sisp<110>}$ $I_{Sisp<10\underline{1}0>}$ $I_{Sisp<1\underline{2}10>}$
Hexagonal (lower) layer: I_{TCSi} I_{Hex} $I_{Hex(CSi)}$ $I_{Sisp<100>}$ $I_{Sisp<110>}$ $I_{Sisp<10\underline{1}0>}$ $I_{Sisp<1\underline{2}10>}$

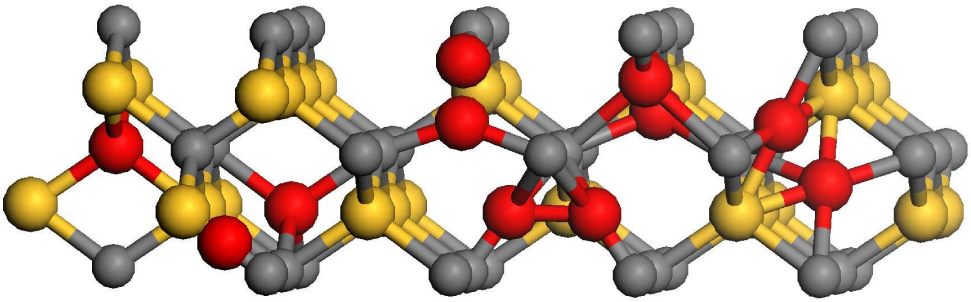

128x52mm (352 x 352 DPI)

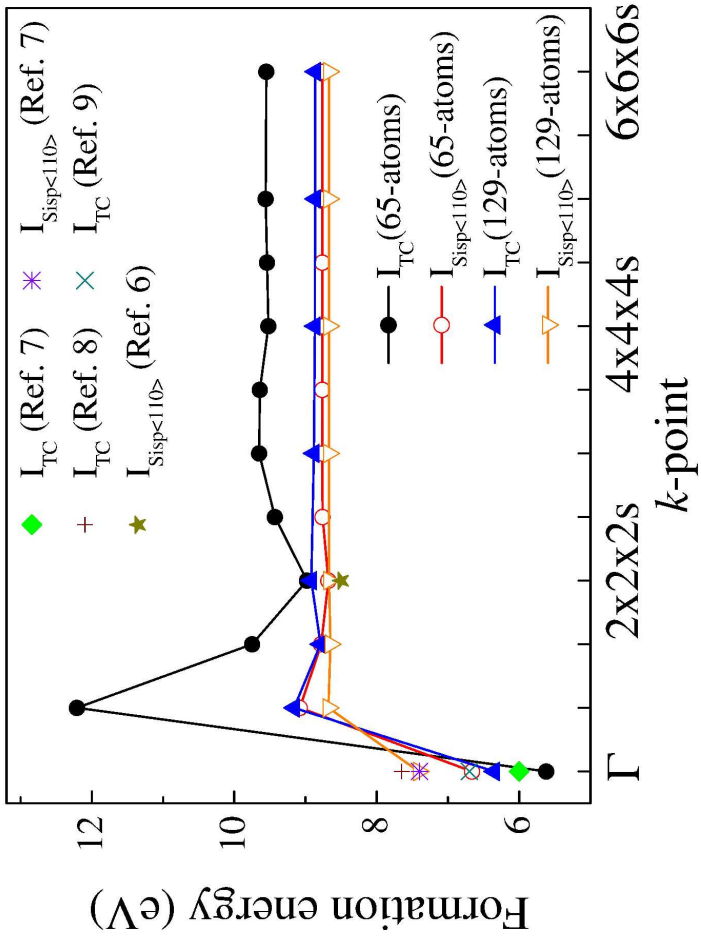

209x297mm (600 x 600 DPI)

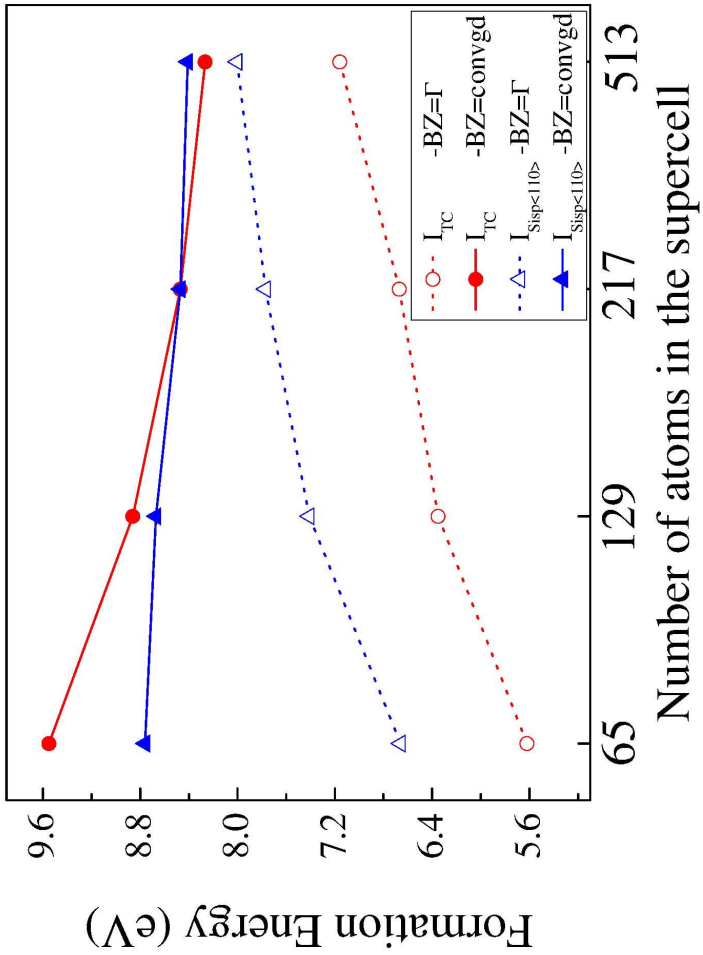

209x297mm (600 x 600 DPI)

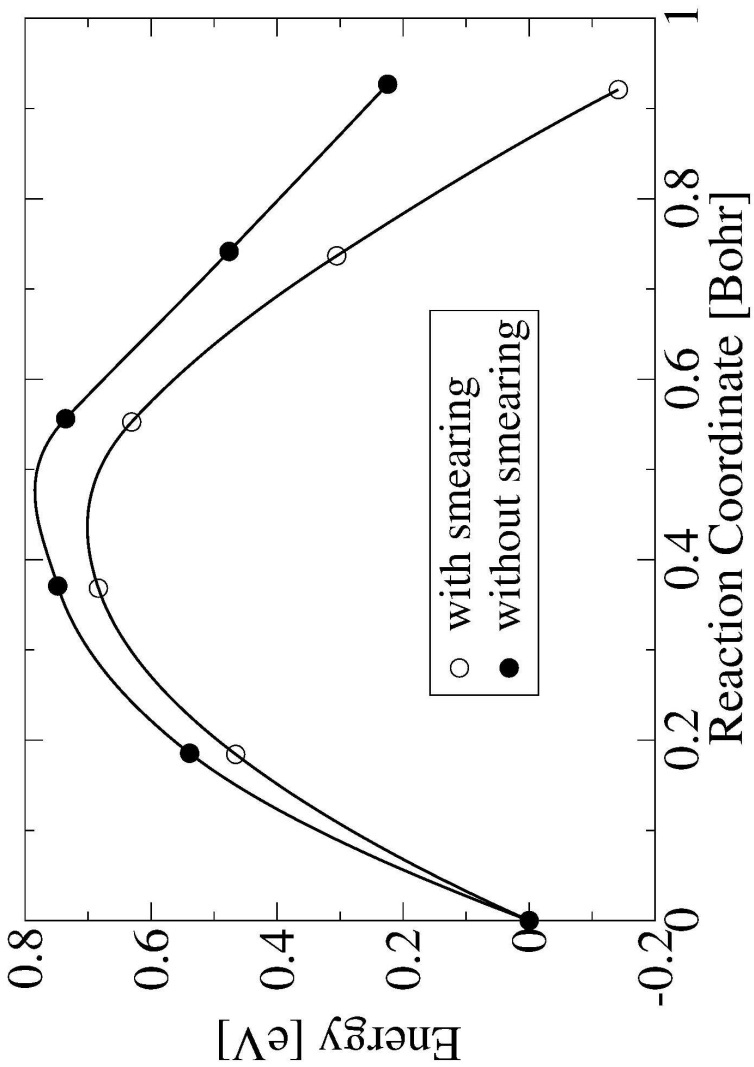

215x279mm (600 x 600 DPI)

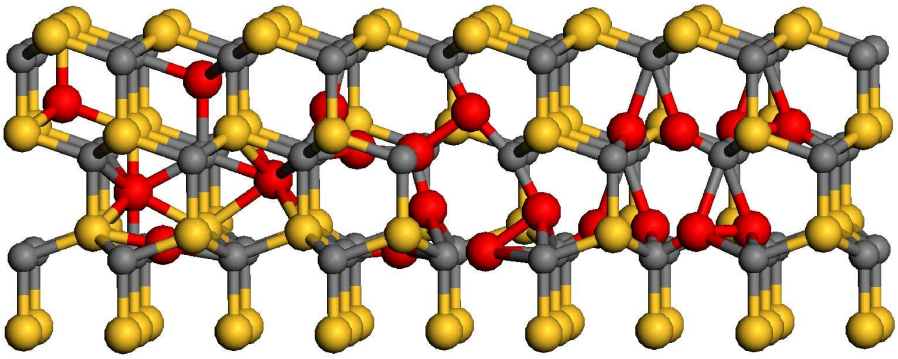

135x58mm (322 x 322 DPI)